

Article

Effect of Immersion Time in Chloride Solution on the Properties of Structural Rebar Embedded in Alkali-Activated Slag Concrete

Willian Aperador ¹, Jorge Bautista-Ruiz ^{2,*} and Jorge Sánchez-Molina ²¹ Department of Engineering, Universidad Militar Nueva Granada, Bogotá 110111, Colombia² Centro de Investigación de Materiales Cerámicos, Universidad Francisco de Paula Santander, San José de Cúcuta 540003, Colombia

* Correspondence: jorgebautista@ufps.edu.co

Abstract: The electrochemical impedance spectroscopy (EIS) technique is widely used in the study of the corrosion of metallic materials. This method also allows for the electrical characterization at the ceramic–metal interface in contact with an aqueous solution composed of chloride ions. EIS makes it possible to discriminate the contribution of the phenomena that occur in the interface to determine the porosity of the cementitious material. The porosity determines the degree of corrosion of the metallic material and the diffusion processes on the electrode surface. In this study, the degradation of a type of non-Portland cement obtained from blast furnace steel slag and activated alkali was evaluated. This type of cement is of great interest because it avoids the emission of CO₂ during its manufacture. Estimating the porosity determined the degree of deterioration suffered by the steel embedded in the concrete as a function of the evaluation time. The hydrated samples were also characterized by ²⁹Si magic angle spinning nuclear magnetic resonance (MAS-NMR) to determine the structure of the formed calcium silicate hydrate (C-S-H) gel. This mixture formed a C-S-H gel, constituted mainly of silicon in the middle groups, in chains in the disilicates. The effect of the slag was remarkable in improving the other evaluated characteristics, i.e., in the porous matrix, the concrete was found to significantly reduce the current passing through as a function of time, showing a reduction in porosity and an increase in impedance because of the generated pozzolanic reaction.

Keywords: porosity; EIS; corrosion; alkali-activated slag; diffusion

Citation: Aperador, W.; Bautista-Ruiz, J.; Sánchez-Molina, J. Effect of Immersion Time in Chloride Solution on the Properties of Structural Rebar Embedded in Alkali-Activated Slag Concrete. *Metals* **2022**, *12*, 1952. <https://doi.org/10.3390/met12111952>

Academic Editor: Renato Altobelli Antunes

Received: 11 October 2022

Accepted: 11 November 2022

Published: 15 November 2022

Publisher's Note: MDPI stays neutral with regard to jurisdictional claims in published maps and institutional affiliations.



Copyright: © 2022 by the authors. Licensee MDPI, Basel, Switzerland. This article is an open access article distributed under the terms and conditions of the Creative Commons Attribution (CC BY) license (<https://creativecommons.org/licenses/by/4.0/>).

1. Introduction

There is extensive scientific information on the potential of alkali-activated concrete as a sustainable material to replace ordinary Portland cement due to its low energy cost, high compressive strength, rapid setting and hardening, and its resistance to fire, acid, and saline solutions compared to ordinary Portland cement [1]. However, the electrochemical characteristics of the concrete–steel system have become the subject of recent studies due to the valuable life guaranteed—for at least 50 years—for structures built with reinforced concrete [2]. These are the challenges facing developers and marketing agencies engaged in large-scale construction [3].

Alternative types of cement are obtained by mixing different minerals, residues, and industrial by-products [4]. These materials, on some occasions, do not meet the specifications to be classified as materials suitable for incorporation into cement and concrete [5]. However, using alkaline activation technology, industrial waste and by-products can be transformed into new materials with low energy consumption, high durability, and excellent mechanical performance [6,7]. A specific type of said cement is obtained from blast furnace steel slag, which uses a relatively simple preparation of materials [8]. The metallurgical industry generates considerable amounts of this industrial “waste”, but it is not correctly used [9]. Therefore, studying blast furnace slag as a raw

material for manufacturing new cement is of great scientific, environmental, and economic interest [10]. The research results aimed at characterizing these materials can benefit both slag-producing companies and those that manufacture construction materials [11]. The former companies can improve the disposal of their waste with less environmental impact. From the low-cost slag, the latter companies will obtain cement with excellent mechanical, durability, and preparation properties [12].

Reinforced concrete is one of the most versatile construction materials, due both to its properties regarding its service and wide range of applications, as well its low cost [12]. However, the reinforcing steel in this structure is susceptible to corrosion, considerably reducing the useful life of structures built with this type of material [13,14].

In this study, the degradation of a type of non-Portland cement obtained from blast furnace steel slag and activated alkali was evaluated. This type of cement is of great interest because it avoids the emission of CO₂ during its manufacture. Estimating the porosity determined the degree of deterioration suffered by the steel embedded in the concrete as a function of the evaluation time. The hydrated samples are also characterized by ²⁹Si magic angle spinning nuclear magnetic resonance (MAS-NMR) to determine the structure of the formed calcium silicate hydrate (C-S-H) gel. This mixture formed a C-S-H gel, constituted mainly of silicon in the middle groups, in chains in the disilicates. The effect of the slag was remarkable in improving the non-Portland cement, i.e., in the porous matrix, the concrete was found to considerably reduce the current passing through as a function of time, showing a reduction in porosity and an increase in impedance because of the generated pozzolanic reaction.

2. Materials and Methods

2.1. Preparation of Concrete Specimen

The study mixtures were obtained by cementing granulated blast furnace slag activated with sodium silicate (Na₂SiO₃) at a 5% Na₂O, expressed as a percentage by slag weight to be incorporated. The SiO₂/Na₂O ratio used was 2.4. The manufacture of the concrete mixtures in both cases contained a cementitious material dosage of 300 kg/m³. It was assumed that the water + activator/slag solution ratios were equivalent; the ratio was 0.5 to obtain an adequate slump of 80 mm.

The type, composition, and size of the fine and coarse aggregates corresponded to gravel with a maximum size of 19 mm, a specific gravity of 2.94 g/cm³, a compact unit mass of 1860 g/cm³, a loose unit mass of 1700 g/cm³, and an absorption of 1.3%. The sand employed in the mixture had a specific surface area of 2.47 g/cm³, a compact unit mass of 1670 g/cm³, a loose unit mass of 1580 g/cm³, and an absorption of 2.9%. Curing was carried out with a relative humidity of approximately 85% and a constant temperature of 25 °C.

2.2. Microstructural Characterization

The microstructural characteristics of the materials were also studied via ²⁹Si magic angle spinning nuclear magnetic resonance (MAS-NMR) at the age of 90 days. Solid-state ²⁹Si MAS-NMR spectra were recorded using a Bruker Avance-400 pulse spectrometer. Spectra were recorded after irradiation of the samples with a $\pi/2$ (5- μ s) pulse; the resonance frequency used was 79.5 MHz, (9.4 T magnetic field), and the spinning rate was 10 kHz. In order to avoid saturation effects, the recycle delay time was set at 10 s. All measurements were taken at room temperature with TMS (tetramethylsilane) as the external standard. The error in chemical shift values was estimated to be lower than 0.5 ppm. NMR spectra deconvolutions were performed using the DMFIT software [15]. Chemical shift (position of the line), intensity (integrated area), width (width at half-height), and line shape (Lorentzian or Gaussian) of the components were then deduced.

2.3. Immersion Test

The samples for the study were manufactured using the materials specified above and were arranged as shown in Figure 1. For the development of the electrochemical tests, Cu/CuSO₄ (sat) electrodes were used as external reference electrodes. The working electrode corresponds to a reference structural steel ASTM A706 commonly used in earthquake-resistant constructions, with a diameter of 1/8" and without any previous treatment.

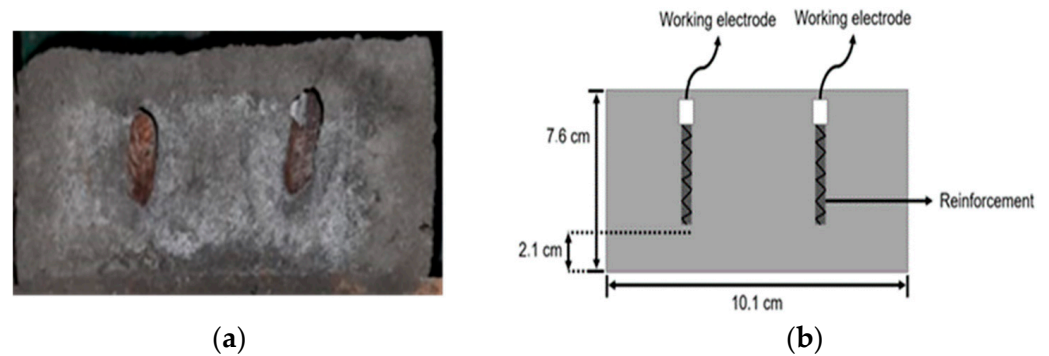


Figure 1. Reinforced concrete used in determining the effect of porosity and its correlation with degradation: (a) sample; (b) schematic.

The samples with the reinforcing steel were immersed in a liquid solution saturated with 3.5% analytical sodium chloride (Panreac PA 131655.1211 NaCl-99.0%), and cycles of agitation of the liquid solution were carried out every 28 days. Due to the evaporation process that occurs, the solution was analyzed and stabilized to the original salt content in order to maintain the initial conditions. This solution then acts as the electrolyte of the electrochemical cell, which was located in a climate controlled environment at 20 °C with a relative humidity of 60%, where it was left to stand for 60 min after carrying out the connections of the assembly in order to avoid distortions during the measurements performed during testing.

2.4. Electrochemical Test

Over the nine-year period, the steel's behavior was monitored using the electrochemical impedance spectroscopy (EIS) technique to determine the characteristics of the concrete–steel interface. The study configuration is shown in Figure 2. The characterization was performed with a Gamry Interface 1010 ETM potentiostat/galvanostat. A 10-mV sinusoidal signal was applied in one sweep at frequencies ranging from 10⁵ Hz to 10^{−3} Hz. The modeling of the equivalent electrochemical circuits was carried out with the Echem Analyst software.

2.5. Durability Properties

The properties of water absorption, including total porosity, were evaluated using cylindrical specimens with a diameter of 76.2 mm and a thickness of 50 mm, according to the standard procedure described in ASTM C642-06 [16]. In addition, the resistance to chloride ion penetration was determined through the Rapid Chloride Permeability Test (ASTM C1202-05) by measuring the passage of an electric current through the chloride ion. [17].

2.6. Chloride Migration

The NT Build 492 standard was used to determine the non-steady state chloride migration coefficient in concrete or cement-based materials [18]. The standard requires hardened samples to determine the material's resistance to chloride penetration. The method requires samples with a diameter of 100 mm and a thickness of 50 mm cut from the casting cylinders. The samples are immersed in a saturated solution of calcium hydroxide—Ca(OH)₂—and prepared with distilled water, using a desiccator and a vacuum pump, for

25 h. Once the saturation cycle is complete, the anode contains a 0.3 N NaOH solution (12 g NaOH in 1000 mL distilled water), and the cathode contains a 2 N NaCl solution (100 g NaCl in 900 mL water).

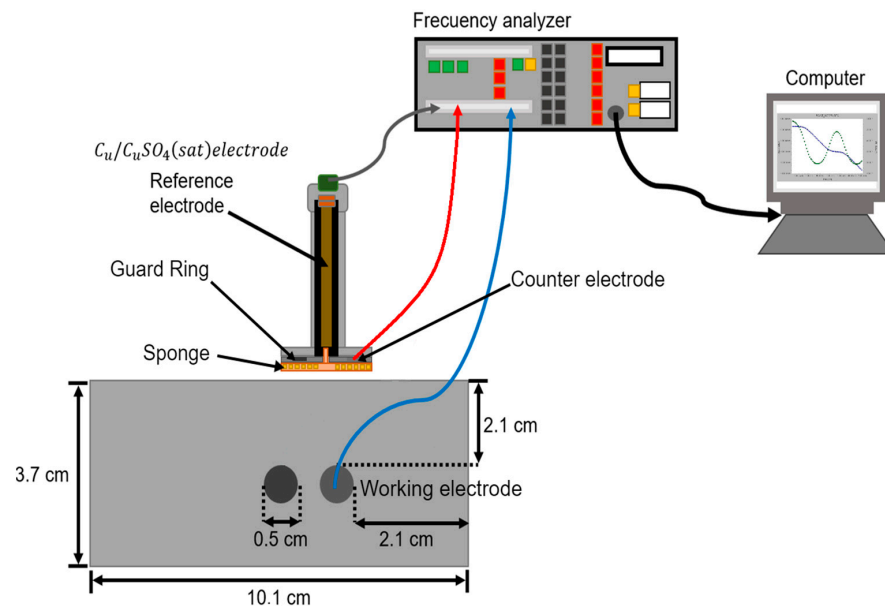


Figure 2. Experimental setup for the characterization of reinforced concrete samples.

3. Results and Discussion

3.1. Microstructural Characterization

The ^{29}Si NMR spectra of the blast-furnace slag are shown in Figure 3, and the deconvolutions of the starting materials are listed in Table 1. The ^{29}Si spectrum of the anhydrous cement showed 5 peaks; the peaks at -57 , -71 , -80 , and -91 are assigned to the glassy component of the slag, and these signals confirmed the presence of natural pozzolans. The last peak in the spectrum is a very wide signal, which is indicative of low crystallinity. The gehlenite -71 ppm signals were still observed. The two signals of the natural pozzolan (-80.3 and -90.8 ppm) were also detected; this implies that the pozzolan is a non-reactive material, as its percentage was maintained after the hydration of the cement, and the peak at -89 ppm corresponded to the crystalline mullite [14]. The signal assigned to the Q4(0Al) units remained very wide, but had shifted slightly downward (greater chemical shift) and was centered at -106 ppm.

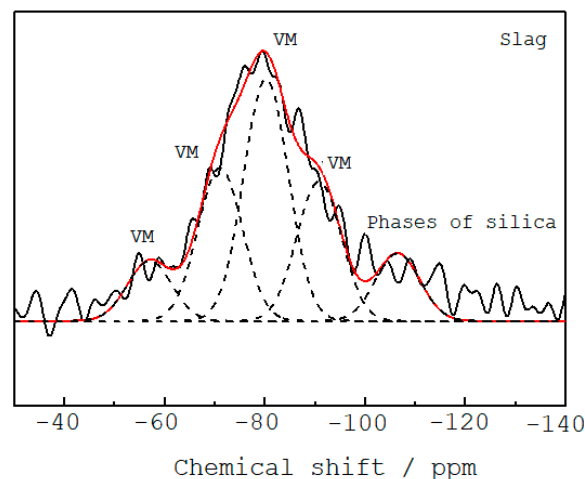


Figure 3. ^{29}Si NMR spectra of the raw materials.

Table 1. Deconvolution of the ²⁹Si MAS-NMR spectra.

Slag	Position (ppm)	Vitreous Material				Phases of Silica, Q ⁴ (0Al)
		−57.1	−71.1	−80.3	−90.8	−106.5
	Width	10.49	10.49	10.49	10.49	10.49
	Integral (%)	9.11	23.13	36.50	21.05	10.22

3.2. Electrochemical Impedance Spectroscopy

Figure 4 shows the equivalent circuit characterized by the resistors and CPEs (constant phase elements) used in the impedance data simulation, indicating the distribution of the ions in the sample-solution system. The first interface corresponds to cementitious material in contact with the saline solution (R_s combined with Y_{p1}-R₁). The second corresponds to the cementitious material containing the reinforcing steel (R₁-Y_{p1}) combined with Y_{p2}-R₂.

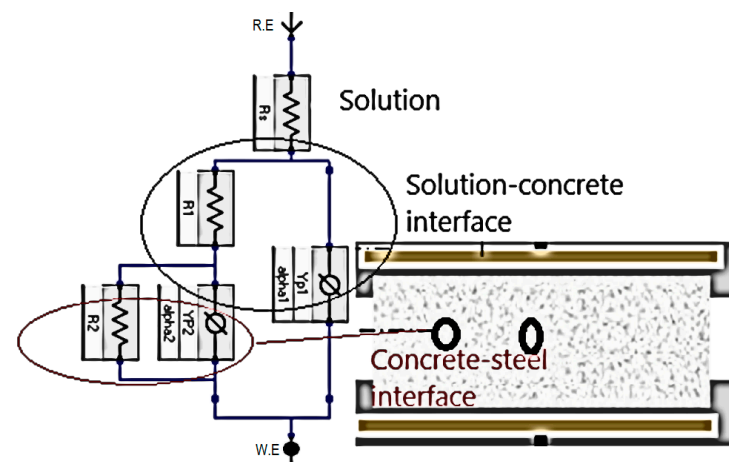


Figure 4. Equivalent circuit corresponding to the different interfaces.

Figure 5 shows the Bode plots as a function of time for the alkaline-activated concrete samples immersed in a 3.5% sodium solution. Table 2 includes the parameters used in the simulation. The values of these parameters have been obtained using a complex least-square nonlinear program (CNLS) [19]. In addition, the EIS test allows the diffusion coefficient to be calculated and the degree of porosity of the material to be related [20]. Finally, the Bode plots have been simulated using the equivalent electrical circuit in Figure 3.

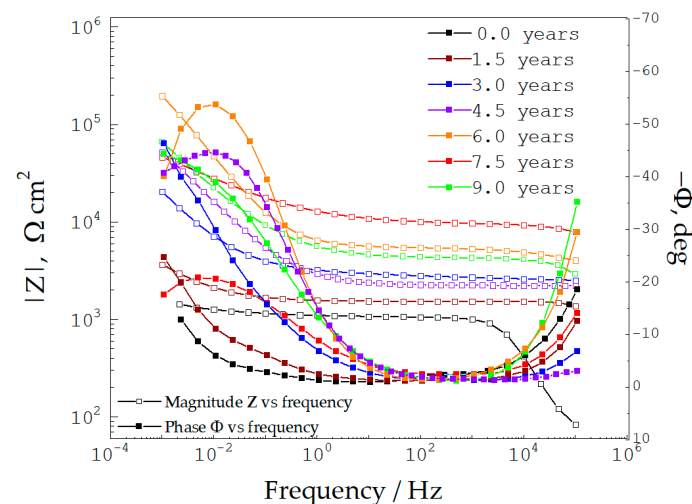


Figure 5. Bode plots for steel samples embedded in concrete and evaluated over a nine-year period.

Table 2. Values of the characteristic parameters used in evaluating the behavior of steel embedded in alkaline-activated concrete, along with its response over time.

Time Years	R_s $\Omega \text{ cm}^2$	R_1 $\text{k}\Omega \text{ cm}^2$	Y_{P1} $\mu\text{F}/\text{cm}^2 \text{ s}^{1-\alpha_1}$	α_1	Y_{P2} $\mu\text{F}/\text{cm}^2 \text{ s}^{1-\alpha_2}$	α_2	R_2 $\text{k}\Omega \text{ cm}^2$
0	7.27	0.82	385	0.8421	12	0.8214	1.425
1.5	8.31	1.357	563	0.8448	45	0.7953	3.602
3	12.21	2.158	474	0.8718	58	0.6399	20.316
4.5	25.14	2.479	465	0.8932	69	0.7563	56.521
6	28.65	8.869	1274	0.8510	235	0.6954	189.350
7.5	39.21	3.953	622	0.8714	157	0.7369	63.872
9	48.97	5.77	653	0.8845	155	0.7152	69.233

In the Bode plots, as a function of the evaluation time (Figure 4), a capacitive behavior is observed by two time-constants determined by two flattened mid- and low-frequency inflections in which the center is located below the real axis [21]. The inflection defined at high frequencies is associated with the porosity of the samples [22]. This phenomenon of lower inflection attenuation is associated with a dispersion process in the frequency, since the surface of the steel rod is corrugated. The phase vs. frequency Bode plots define an inflection at high frequencies after 3 years of evaluation. This type of behavior can be interpreted by the barrier effect generated in the system, being more significant at 6 years and stabilizing at 7.5 years [23,24].

The Bode plots showing magnitude vs. frequency (Figure 5) show the evolution of the concrete's protective effect over time when immersed in a solution of 3.5% by weight of NaCl. For 1.5 years, the value of the magnitude of impedance doubled regarding the material after the curing process and without the presence of a chloride ion. This condition was called zero time. Subsequently, the impedance values increased dramatically up to the 6-years point [25]. After 7.5 years of testing, the magnitude of the impedance decreased, stabilizing, and the values were like those obtained at 9 years [26]. The results showed that the impedance values increased in the first years of the test due to the alkaline activation of the aluminosilicates, which played an essential role in the stability of the steel. After the sixth year of testing, the decomposition of the steel's protective layer was accelerated, similar to the behavior noted without protection; the loss of stability was minimal after 7.5 years, and there was no evidence of a decrease in impedance values [27].

The evolution of the impedance occurs in the first 28 days of concrete curing, during which time the formation of the hydration products of the pozzolanic reaction favors the initial values of protection against the corrosion phenomena [28]. Likewise, the samples in contact with the NaCl solution evaluated between 18 months and 9 years showed that the impedance values were related to the decrease in the degree of porosity of the mixtures. This process is attributed to a higher generation of hydration products as a result of the protection of steel. Using materials such as iron and steel slag in concrete mixtures contributes to the optimization of the mechanisms that control the entry of chloride ions into the samples [29]. Using materials such as iron and steel slag in concrete mixes helps optimize the mechanisms that control the entry of chloride ions into the samples [29]. Blast furnace slag, with its pozzolanic, chemical, and physical properties, can reduce the permeability of mixtures during their hydration processes. These characteristics prevent the migration of chloride ions into the samples, improving their durability [30]. Alkaline activation generates dense and uniform zones at the steel-concrete interface owing to the slag activated with Na_2SiO_3 . This behavior is attributed to factors such as the water content that reduces the function of Na_2SiO_3 . The low porosity as a function of time is explained by the high initial concentrations of SiO_4 in the pore solution and the increasing dissolution of quartz [31]. Another factor is the production of calcium hydroxide in the cementitious hydration processes, resulting in the formation of hydrated calcium silicates that fill the existing pores in the concrete mixtures, reducing porosity [32,33].

The impedances shown in Figure 5 illustrate the different assessment times, indicating that when compared to the average migration of the chloride ion in the concrete, the first years of evaluation show that the reaction was slow, and the migration values were high. However, after 7.5 years of evaluation, it was established that the pozzolanic activity generated a reduction in the migration of the chlorides. Therefore, time was determined to be a factor in reducing the mobility of the chloride ions across the porous matrix.

3.3. Resistance to Chloride Ion Penetration

Figure 6 shows the results obtained by applying the ASTM C1202 standard to determine the permeability of concrete to chloride ions. This methodology measures the passage of an electrical current through concrete samples [31,32]. The behavior of the analyzed concretes as a function of the transferred load is observed (Figure 6). The results show that the alkali-activated concrete evaluated for up to 9 years presented a lower permeability to chlorides than did the samples at 28 days, which was called zero value. Slag concrete activated with sodium silicate is classified as having a low permeability to chlorides, and the behavior is observed as a function of time, up to nine years [33]. This behavior is associated with the plugging of the pores. The permeability of concrete is explained by the relationship or factor that most influences the fixation of chloride ions to the sample. The high concentration of chlorides in the studied systems is due to the exposure time (nine years), which can increase the capacity of the sample to fix chlorides [34]. It was also determined that the concretes evaluated at nine years could still fix chlorides; therefore, the existence of free chloride ions (within the concrete samples) looking for a way to fix themselves to the specimens was noted. These free chloride ions can affect the durability of concrete because they are responsible for initiating the corrosive process in the steel reinforcement within the structures [35]. By correlating this phenomenon with the EIS technique, it was established that the high impedance values are due to the presence of alumina in activated concrete, which is associated with the ability of concrete mixtures to fix and immobilize free chloride ions within the pore solution [36].

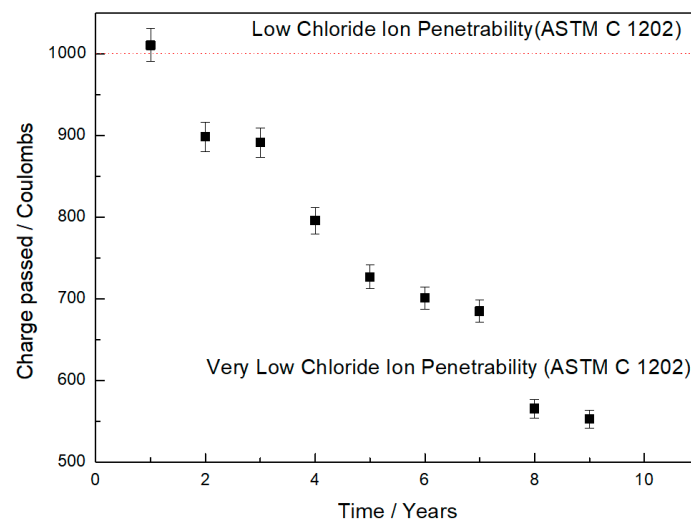


Figure 6. Determination of resistance to chloride ion penetration.

3.4. Volume of Permeable Pores

Figure 7 shows the results obtained for the concrete used in this study, based on the volume of permeable pores. In the graph, the concretes with more exposure time to the saline solution had fewer permeable pores [37]. That is, they are good quality concretes. In the case of alkali-activated iron and steel slag concrete, this property is attributed to the more significant densification of the paste—due to the presence of the hydration products—along the evaluation times, generating a lower percentage of pores [38]. This behavior is compared with the results obtained by chloride ion permeability and electrochemical

impedance spectroscopy, since chloride ions can be absorbed or dissolved in the water concentrated in the pores. As previously mentioned, free chlorides are responsible for the corrosion of the steel used to reinforce concrete structures. However, the low volume is associated with the hydration of the cement, so there is no corrosion promoter [39]. This behavior is attributed to the reactivity of the granulated blast furnace slag in the presence of the alkaline activator, causing hydration products that block the pores, resulting in slower chloride ion ingress rates when evaluating the systems as a function of time [40].

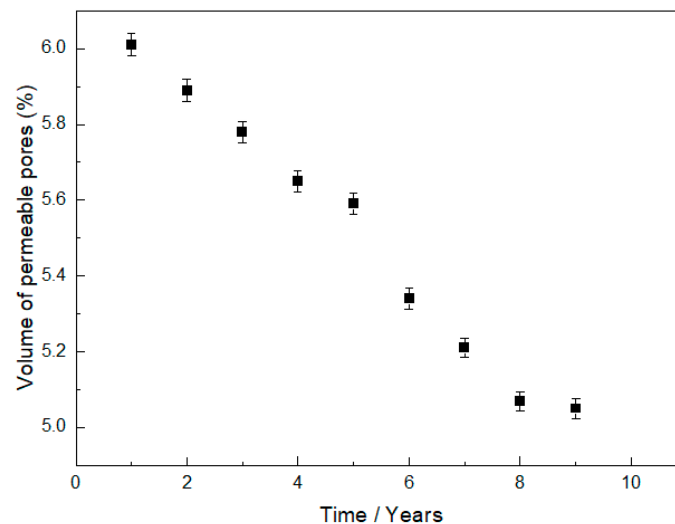


Figure 7. Variation of permeability in concrete with alkaline activation.

3.5. Chloride Ion Migration

Figure 8 shows the average evaluation times of chloride ion migration in concrete. The graph shows high values in the first years of evaluation. However, after the third year of evaluation, it was determined that the pozzolanic activity reduces the migration of chlorides. From the analysis, it can be concluded that the mobility of the chloride ions through the porous matrix is reduced over time.

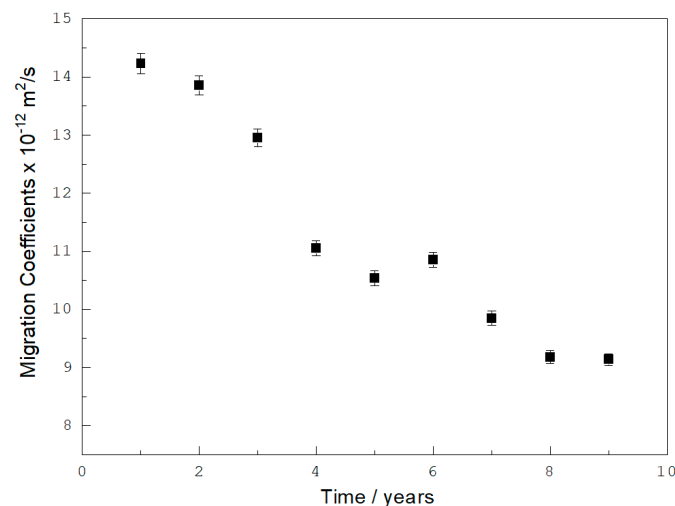


Figure 8. Non-steady-state migration coefficient as a function of time.

3.6. X-ray Diffraction

Figure 9 shows the X-ray diffraction results of the corrosion product characterization once the electrochemical studies have been completed. The procedure consisted of longitudinally cutting the specimens at immersion times of 0, 1.5, 3, 6, and 9 years to study the

concrete–steel interface. The spectra in Figure 7 show crystalline quartz (SiO_2), C-S-H formation (CS), calcium carbonate (C), and beta larnite corresponding to Ca_2SiO_4 . The corrosion products identified on the steel surface correspond to compounds such as brownmillerite related to CaAlFeO , goethite, magnetite, fayalite, iron oxyhydroxides, and hematite. These compounds are related to iron oxides and hydroxides in all the samples analyzed.

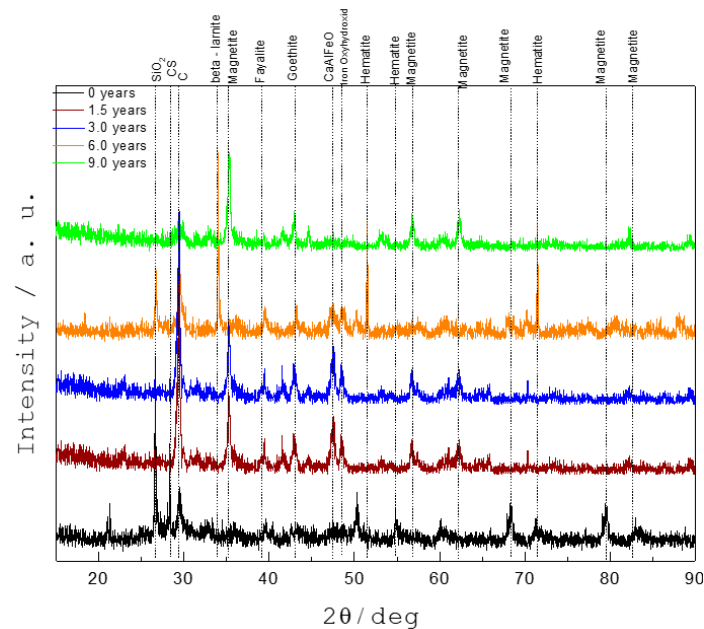


Figure 9. The X-ray diffraction patterns of the concrete–steel interface.

Additionally, the ray diffraction results for the alkali-activated slag concrete samples experiencing at least 1.5 years or more of saline solution immersion time showed overlapping characteristic diffraction peaks. The same intensity values were observed for the calcium silicate-hydrate phase at 28.52° and calcium carbonate at 29.46° . It is also evident that the samples evaluated after up to three years of immersion in the saline solution showed a higher intensity peak due to the stability of the layer of cementitious material present in the steel–concrete interface. This layer was not removed by the pH present in the concrete. When the concrete samples are subjected to salt immersion, the influx of chloride ions accelerates the removal of the oxide layer. The removal degree of the oxides is directly related to the exposure time of the samples to the solution [41]. However, the passivating layer was determined with EIS measurements (Figure 4). The impedance values indirectly indicate the formation of a protective passivating layer over the steel.

The study determined that the corrosion products found on the steel surface are the phases corresponding to iron oxides, especially the ones corresponding to the fayalite $\text{Fe}_2(\text{SiO}_4)$ at 39.17° formed in the electrochemical reactions. Magnetite compounds ($\text{FeO}\cdot\text{Fe}_2\text{O}_3$, $\text{Fe}^{2+}\text{Fe}^{3+}_2\text{O}_4$) with peaks located at 35.19° ; 56.90° ; 62.20° ; 68.37° ; 79.50° , and 82.58° , and hematite ($\alpha\text{-Fe}_2\text{O}_3$), with peaks at 51.40° , 54.91° , and 71.46° , were also noted. These products arise from the reaction process, as well as during the manufacture of steel; they are known as the “steel shell”, but they offer low anticorrosive protection. The protective layer is mainly formed by iron oxyhydroxides (48.51°), transforming into a mixture of hydroxides and goethite (42.97°). Although this iron oxide has excellent chemical stability, it has an irregular morphology and protects the steel against electrochemical attacks. In addition, compounds such as magnetite and hematite increase the thickness of the oxide layer, forming a mechanical protective barrier (small scale) [42,43]. Finally, the thick passive layer formed with low protection compounds (iron oxyhydroxides and goethite), the electrochemical stability of the steel, and the low porosity of the concrete generate more excellent anticorrosive protection of the steels embedded in concretes based on activated slag.

4. Conclusions

This work used alkali-activated slag as a raw material to obtain concrete. Monosilicates (Si-OH) and Al-OH groups then formed, which facilitated the polymerization of the silicate chains in the C-S-H gel. These species connected the C-S-H dimers, producing a C-S-H gel richer in Al. This compound contributes to optimizing the mechanisms that control the entry of chlorides into the mixture, reducing the permeability of the concrete during the hydration processes and favoring protection against electrochemical attacks.

It was also established that the protection mechanism in slag concrete improved when it was immersed in saline solution, which evaluated as a function of time. Furthermore, the protection of metal immersed in the concrete is related to the formation of oxide (and hydroxide) layers on the steel due to the low degree of porosity of the samples.

The impedance data increased up to 6 years, and its stabilization at 7.5 years is explained by the simultaneous combination of the uniform formation of protective layers on the steel surface and the restriction of the passage of harmful elements into the system through the ceramic matrix.

Author Contributions: Conceptualization, W.A. and J.B.-R.; methodology, J.S.-M.; software, W.A.; validation, J.B.-R.; formal analysis, J.S.-M.; investigation, W.A. and J.B.-R. All authors have read and agreed to the published version of the manuscript.

Funding: This research work was funded by Vicerrectoria de Investigaciones Universidad Militar Nueva Granada through the INV_ING_3123 project.

Institutional Review Board Statement: Not applicable.

Data Availability Statement: Not applicable.

Acknowledgments: W. Aperador acknowledges support from the Universidad Militar Nueva Granada.

Conflicts of Interest: The authors declare no conflict of interest.

References

- Schneider, N.; Stephan, D. Reactivation of a Retarded Suspension of Ground Granulated Blast-Furnace Slag. *Materials* **2016**, *9*, 174. [[CrossRef](#)] [[PubMed](#)]
- Mujahid-Amran, H.S.; Abdelgader, A.M.; Onaizi, R.F.; Today-Ozbakkaloglu, R.S.M.; Rashid, G. 3D-printable alkali-activated concretes for building applications: A critical review. *Constr. Build. Mater.* **2022**, *319*, 126126. [[CrossRef](#)]
- Mengasini, L.; Mavroulidou, M.; Gunn, M.J. Alkali-activated concrete mixes with ground granulated blast furnace slag and paper sludge ash in seawater environments. *Sustain. Chem. Pharm.* **2021**, *20*, 100380. [[CrossRef](#)]
- Criado, M.; Aperador, W.; Sobrados, I. Microstructural and Mechanical Properties of Alkali Activated Colombian Raw Materials. *Materials* **2016**, *9*, 158. [[CrossRef](#)] [[PubMed](#)]
- Jin, Z.; Zhao, X.; Du, Y.; Yang, S.; Wang, D.; Zhao, T.; Bai, Y. Comprehensive properties of passive film formed in simulated pore solution of alkali-activated concrete. *Constr. Build. Mater.* **2022**, *319*, 126142. [[CrossRef](#)]
- Tahri, W.; Hu, X.; Shi, C.; Zhang, Z. Review on corrosion of steel reinforcement in alkali-activated concretes in chloride-containing environments. *Constr. Build. Mater.* **2021**, *293*, 123484. [[CrossRef](#)]
- Ibrahim, M.; Abiodun, B.; Algaifi, H.; Rahman, M.; Nasir, M.; Ewebajo, A. Assessment of acid resistance of natural pozzolan-based alkali-activated concrete: Experimental and optimization modelling. *Constr. Build. Mater.* **2021**, *304*, 124657. [[CrossRef](#)]
- Fořt, J.; Mildner, M.; Koppert, M.; Černý, R. Waste solidified alkalis as activators of aluminosilicate precursors: Functional and environmental evaluation. *J. Build. Eng.* **2022**, *54*, 104598. [[CrossRef](#)]
- Kumar-Das, S.; Adediran, A.; Rodrigue-Kaze, C.; Mohammed-Mustakim, S.; Leklou, N. Production, characteristics, and utilization of rice husk ash in alkali-activated materials: An overview of fresh and hardened state properties. *Constr. Build. Mater.* **2022**, *345*, 128341. [[CrossRef](#)]
- Amran, M.; Al-Fakih, A.; Chu, S.H.; Fediuk, R.; Haruna, S.; Azevedo, A.; Vatin, N. Long-term durability properties of geopolymer concrete: An in-depth review. *Case Stud. Constr. Mater.* **2021**, *15*, e00661. [[CrossRef](#)]
- Ibrahim, M.; Maslehuddin, M. An overview of factors influencing the properties of alkali-activated binders. *J. Clean. Prod.* **2021**, *286*, 124972. [[CrossRef](#)]
- Amran, M.; Fediuk, R.; Abdelgader, H.; Murali, G.; Yong, Y. Fiber-reinforced alkali-activated concrete: A review. *J. Build. Eng.* **2022**, *45*, 103638. [[CrossRef](#)]
- Kathirvel, P.; Mohan-Kaliyaperumal, S.R. Influence of recycled concrete aggregates on the flexural properties of reinforced alkali-activated slag concrete. *Constr. Build. Mater.* **2016**, *102*, 51–58. [[CrossRef](#)]

14. Aperador, W.; Mejía de Gutiérrez, R.; Bastidas, D.M. Steel corrosion behaviour in carbonated alkali-activated slag concrete. *Corros. Sci.* **2009**, *51*, 2027–2033. [[CrossRef](#)]
15. Massiot, D.; Fayon, F.; Capron, M.; King, I.; Le Calvé, S.; Alonso, B.; Durand, J.O.; Bujoli, B.; Gan, Z.; Hoatson, G. Modelling one- and two-dimensional solid-state NMR spectra. *Magn. Reson. Chem.* **2002**, *40*, 70–76. [[CrossRef](#)]
16. *ASTM C642-21(2022)*; Standard Test Method for Density, Absorption, and Voids in Hardened Concrete. ASTM International: West Conshohocken, PA, USA, 2021.
17. *ASTM C1202-22(2022)*; Standard Test Method for Electrical Indication of Concrete's Ability to Resist Chloride Ion Penetration. ASTM International: West Conshohocken, PA, USA, 2022.
18. *NT BUILD 492 (1999)*; Concrete, Mortar and Cement-Based Repair Materials: Chloride Migration Coefficient from Non-steady-state Migration Experiments. NORDTEST: Finland, Norway, 1999.
19. Zic, M.; Pereverzyev, S. Optimizing noisy CNLS problems by using Nelder-Mead algorithm: A new method to compute simplex step efficiency. *J. Electroanal. Chem.* **2019**, *851*, 113439. [[CrossRef](#)]
20. Shen, L.; Zhang, H. Corrosion inhibition and adsorption behavior of (3-aminopropyl)-triethoxysilane on steel surface in the simulated concrete pore solution contaminated with chloride. *J. Mol. Liq.* **2022**, *363*, 119896. [[CrossRef](#)]
21. Yang, H.; Xiong, C.; Liu, X.; Liu, A.; Li, T.; Ding, R.; Shah, S.P.; Li, W. Application of layered double hydroxides (LDHs) in corrosion resistance of reinforced concrete-state of the art. *Constr. Build. Mater.* **2021**, *307*, 124991. [[CrossRef](#)]
22. Biondi, L.; Perry, M.; McAlorum, J.; Vlachakis, C.; Hamilton, A. Geopolymer-based moisture sensors for reinforced concrete health monitoring. *Sens. Actuators B Chem.* **2020**, *309*, 127775. [[CrossRef](#)]
23. Rodrigues, R.; Gaboreau, S.; Gance, J.; Ignatiadis, I.; Betelu, S. Reinforced concrete structures: A review of corrosion mechanisms and advances in electrical methods for corrosion monitoring. *Constr. Build. Mater.* **2021**, *269*, 121240. [[CrossRef](#)]
24. Criado, M.; Sobrados, I.; Bastidas, J.M.; Sanz, J. Corrosion behaviour of coated steel rebars in carbonated and chloride-contaminated alkali-activated fly ash mortar. *Prog. Org. Coat.* **2016**, *99*, 11–22. [[CrossRef](#)]
25. Zhou, X.; Yang, H.; Wang, F. [BMIM]BF₄ ionic liquids as effective inhibitor for carbon steel in alkaline chloride solution. *Electrochim. Acta* **2011**, *56*, 4268–4275. [[CrossRef](#)]
26. Huyen-Vu, T.; Chi-Dang, L.; Kang, G.; Sirivivatnanon, V. Chloride induced corrosion of steel reinforcement in alkali-activated slag concretes: A critical review. *Case Stud. Constr. Mater.* **2022**, *16*, e01112. [[CrossRef](#)]
27. Kaur, H.; Singla, S. Non-Destructive testing to detect multiple cracks in reinforced concrete beam using electromechanical impedance technique. *Mater. Today Proc.* **2022**; in press.
28. Liu, P.; Wang, W.; Chen, Y.; Feng, X.; Miao, L. Concrete damage diagnosis using electromechanical impedance technique. *Constr. Build. Mater.* **2017**, *136*, 450–455. [[CrossRef](#)]
29. Talakokula, V.; Bhalla, S.; Gupta, A. Monitoring early hydration of reinforced concrete structures using structural parameters identified by piezo sensors via electromechanical impedance technique. *Mech Syst. Signal Process* **2018**, *99*, 129–141. [[CrossRef](#)]
30. Da Silva, G.F.; Martini, S.; Moraes, J.C.B.; Teles, L.K. AC impedance spectroscopy (AC-IS) analysis to characterize the effect of nanomaterials in cement-based mortars. *Constr. Build. Mater.* **2021**, *269*, 121260. [[CrossRef](#)]
31. Bai, R.; Zhang, J.; Yan, C.; Liu, S.; Wang, X.; Yang, Z. Calcium hydroxide content and hydration degree of cement in cementitious composites containing calcium silicate slag. *Chemosphere* **2021**, *280*, 130918. [[CrossRef](#)]
32. Ibrahim, M.; Kalimur-Rahman, M.; Megat-Johari, M.A.; Nasir, M.; Adeoluwa-Oladapo, E. Chloride diffusion and chloride-induced corrosion of steel embedded in natural pozzolan-based alkali-activated concrete. *Constr. Build. Mater.* **2020**, *262*, 120669. [[CrossRef](#)]
33. Aguirre-Guerrero, A.M.; Mejía de Gutiérrez, R. Alkali-activated protective coatings for reinforced concrete exposed to chlorides. *Constr. Build. Mater.* **2021**, *268*, 121098. [[CrossRef](#)]
34. Thomas, R.J.; Ariyachandra, E.; Lezama, D.; Peethamparan, S. Comparison of chloride permeability methods for Alkali-Activated concrete. *Constr. Build. Mater.* **2018**, *165*, 104–111. [[CrossRef](#)]
35. Mehta, A.; Siddique, R.; Ozbakkaloglu, T.; Ahmed-Shaikh, F.U.; Belarbi, R. Fly ash and ground granulated blast furnace slag-based alkali-activated concrete: Mechanical, transport and microstructural properties. *Constr. Build. Mater.* **2020**, *257*, 119548. [[CrossRef](#)]
36. Zhang, J.X.; Ma, Y.; Zheng, J.; Hu, J.; Fu, J.; Zhang, Z.; Wang, H. Chloride diffusion in alkali-activated fly ash/slag concretes: Role of slag content, water/binder ratio, alkali content and sand-aggregate ratio. *Constr. Build. Mater.* **2020**, *261*, 119940. [[CrossRef](#)]
37. Ma, Y.; Hu, J.; Ye, G. The pore structure and permeability of alkali-activated fly ash. *Fuel* **2013**, *104*, 771–780. [[CrossRef](#)]
38. Hu, X.; Shi, C.; Shi, Z.; Zhang, L. Compressive strength, pore structure and chloride transport properties of alkali-activated slag/fly ash mortars. *Cem. Concr. Compos.* **2019**, *104*, 103392. [[CrossRef](#)]
39. Gao, X.; Yao, X.; Wang, C.; Geng, C.; Yang, T. Properties and microstructure of eco-friendly alkali-activated slag cements under hydrothermal conditions relevant to well cementing applications. *Constr. Build. Mater.* **2022**, *318*, 125973. [[CrossRef](#)]
40. Runci, A.; Serdar, M. Effect of curing time on the chloride diffusion of alkali-activated slag. *Case Stud. Constr. Mater.* **2022**, *16*, e00927. [[CrossRef](#)]
41. Sun, X.; Liu, J.; Qiu, J.; Wu, P.; Zhao, Y. Alkali activation of blast furnace slag using a carbonate-calcium carbide residue alkaline mixture to prepare cemented paste backfill. *Constr. Build. Mater.* **2022**, *320*, 126234. [[CrossRef](#)]

-
42. Moussadik, A.; Saadi, M.; Diouri, A. Chemical, mineralogical and thermal characterization of a composite alkali-activated binder based on coal gangue and fly ash. *Mater. Today Proc.* **2022**, *58*, 1452–1458. [[CrossRef](#)]
 43. Jae-Kim, M.; Ik-Hwang, W.; Jung-Cho, W. The influence of alkali activators on the properties of ternary blended cement incorporated with ferronickel slag. *Constr. Build. Mater.* **2022**, *318*, 126174. [[CrossRef](#)]